Stochastic magnetization dynamics in single domain particles

S. Giordano, Yannick Dusch, Nicolas Tiercelin, Philippe Pernod, Vladimir Preobrazhensky

Stochastic magnetization dynamics in single domain particles

Stefano Giordano[1,a], Yannick Dusch[1], Nicolas Tiercelin[1], Philippe Pernod[1], and Vladimir Preobrazhensky[1,2]

[1] International Associated Laboratory LEMAC/LICS, IEMN, UMR CNRS 8520, PRES Lille Nord de France, ECLille, 59651 Villeneuve d'Ascq, France
[2] Wave Research Center, Prokhorov General Physics Institute, Russian Academy of Science, 38 Vavilov str., 119991 Moscow, Russia

Abstract. Magnetic particles are largely utilized in several applications ranging from magnetorheological fluids to bioscience and from nanothechnology to memories or logic devices. The behavior of each single particle at finite temperature (under thermal stochastic fluctuations) plays a central role in determining the response of the whole physical system taken into consideration. Here, the magnetization evolution is studied through the Landau-Lifshitz-Gilbert formalism and the non-equilibrium statistical mechanics is introduced with the Langevin and Fokker-Planck methodologies. As result of the combination of such techniques we analyse the stochastic magnetization dynamics and we numerically determine the convergence time, measuring the velocity of attainment of thermodynamic equilibrium, as function of the system temperature.

1 Introduction

Magnetic materials and devices play a central role in modern nanoscience and nanotechnology. In particular, dispersions of single domain ferromagnetic particles have received considerable interest, both for their important applications and their complex and multifaceted experimental response. The behavior of simplest dilute systems was clearly understood in the past [1] with some techniques recently generalized for anisotropic media [2]. Moreover, the experimental results for dense systems were interpreted more recently through superparamagnetic relaxation [3] and dipolar interaction [4] models. One important application realized with dispersions of magnetic particle concerns the magnetorheological fluids. They are colloidal suspensions of magnetic particles that reversibly stiffen under the influence of an applied magnetic field. Typically, the particles are coated with a surfactant for stabilization in a carrier solvent [5].

Colloidal suspensions of particles can be also considered as many-body model systems in condensed matter physics. In fact, the fine particles may represent the macroscopic counterparts of atomic systems. In this context, many ordering phenomena have been observed and modelled: creation of chains, triangular lattices and lamellar structures are just some examples [6]. In single domain magnetic arrays the role of the disorder (positional and orientational), coupled with exchange and dipolar interactions, has been investigated for tayloring materials with desired properties [7]. Recent technologies allow to make use of the self-assembly of floating magnetic particles into ordered structures. The lattice constant and the array simmetry may be easily tuned by the application of external magnetic fields and by using different particle shapes. This is a promising route for the fabrication of tunable photonic band gap materials [8].

Magnetic particles are largely used in the area of bioscience and medicine [9–11]. Many applications can be mentioned: separation processes including purification and immunoassay [12,13], magnetic resonance imaging (MRI) [14,15], drug delivery and targeting [16,17], and hyperthermia [18,19].

Moreover, the possibility to obtain a direct coupling between magnetic and electric properties in physical systems has stimulated a considerable interest [20,21]. In particular, composite assemblages of piezoelectric and magnetostrictive phases have been proposed [22]. Heterostructures based on such materials are very promising from the energetic point of view. In fact, the reorientation of the magnetization in single particles dissipates very low energies and it is appropriate for memories, spintronics and new logic paradigms [23–25]. For example, a ferromagnetic particle based magnetoelectric memory element has been recently proposed: it is composed of a magnetoelastic particle embedded in a piezoelectric matrix [26–28]. Different memory structures have been introduced and discussed in literature as well [29–31]. Magnetic particles have been also employed to realize quantum bits

[a] e-mail: Stefano.Giordano@iemn.univ-lille1.fr

useful for implementing factoring or searching quantum algorithms [32].

The basic element of all previous applications is the single magnetic particle, which may exhibit even if isolated a complex behavior with stimulating physical and mathematical features. This paper is devoted to the analysis of the magnetization dynamics in a magnetic particle at finite temperature. In particular, we numerically determine the convergence time quantifying the rate of attainment of the thermodynamic equilibrium for different particle configurations. This quantity is important for the above discussed applications since it controls the overall response time of all complex multi-particle systems. Moreover, the effect of the temperature on the convergence time is crucial for all storage and elaboration systems, where fluctuations may degrade the quality of signals carrying the information. As a matter of fact, the convergence time of the magnetization vector in memories and spintronic devices represent the switching time used to store or elaborate a single bit and, therefore, it plays a central role from the technical point of view. At the beginning of these investigations the dynamic response and the convergence time were analyzed without considering possible thermal effects [33,34]. In successive important studies the temperature effects were introduced by means of the theory of stochastic processes applied to the statistical mechanics [35–37]. Recently, these techniques have been applied to two-dimensional and three-dimensional distributions of single-domain particles [38,39] and to the dynamics of particles driven by a rotating magnetic field [40–43].

Firstly, in Section 2, we describe the energy function of an ellipsoidal particle, which describes the magnetization orientation in terms of the applied field. To do this we neglect anisotropic, elastic and exchange contributions. It implies that the models examined have a main didactic objective. Nevertheless, the consideration of the thermal bath embedding the particle yields non trivial results of general interest. As for the dynamic of the magnetization direction, the above-mentioned energy function has been combined with classical Landau-Lifshitz-Gilbert (LLG) equation [44–47]. Moreover, in Section 3, we give a brief outline of its generalization with the Brown random field mimicking the thermal effects [48–51]. This approach, as well known, leads to a stochastic Langevin equation or, equivalently, to a Fokker-Planck equation describing the time evolution of the density probability of the magnetization direction [35–37]. Important applications of such techniques concerned single particles and ensembles of interacting and non-interacting particles [38–43]. In this paper, the numerical solution of the Langevin LLG stochastic equation allows us to evaluate the convergence time to the thermodynamic equilibrium. In particular we examine the behavior of the convergence time versus the temperature of the system. Specific results have been obtained for the following configurations: in Section 4, we consider a spherical particle without applied field (in this case the magnetization evolves as a random walk on a spherical surface); in Section 5, we analyse the stochastic dynamics in a sphere under magnetic field and, finally, in Section 6, we consider prolate and oblate ellipsoidal particles corresponding to axial and planar geometrical anisotropies, respectively.

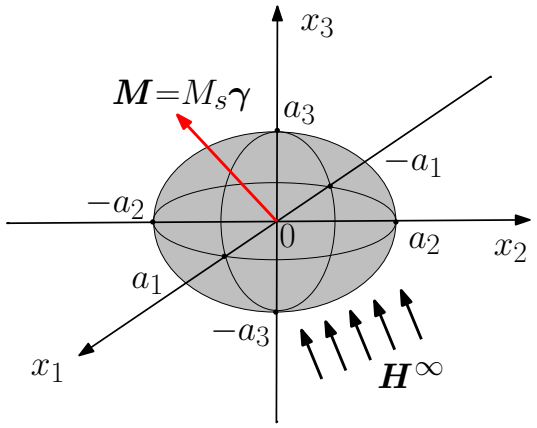

Fig. 1. Ellipsoidal magnetic particle with magnetization $\boldsymbol{M}$ subjected to a magnetic field $\boldsymbol{H}^\infty$.

2 Energy function for ellipsoidal particles

We consider the ellipsoidal particle depicted in Figure 1 and we suppose that its size is small enough to assure the presence of a single ferromagnetic domain. Therefore, an uniform magnetization $\boldsymbol{M} = M_s\,\boldsymbol{\gamma}$ appears where M_s is the magnetization at saturation and $\boldsymbol{\gamma}$ is a unit vector. The orientation $\boldsymbol{\gamma}$ can be obtained by minimizing the energy function as follows:

$$w(\boldsymbol{\gamma}) = -\mu_0 M_s \boldsymbol{\gamma}\boldsymbol{H}. \tag{1}$$

It represents the Zeemann energy and describes the influence of the local magnetic field $\boldsymbol{H}$ on the orientation of $\boldsymbol{\gamma}$. For simplicity, in this work we neglect the following terms of the energy function: (i) the anisotropic energy depending on the actual crystalline structure of the particle, (ii) the elastic energy describing the magnetostriction and, therefore, the mechanical interaction with the matrix where the particle is embedded, and (iii) the exchange energy term describing the magnetic interactions among different domains.

It is important to remark that the minimization furnishes the direction in terms of the magnetic field $\boldsymbol{\gamma} = \boldsymbol{\gamma}(\boldsymbol{H})$. The constitutive equation of the particle is given by $\boldsymbol{B} = \mu_0(\boldsymbol{H} + M_s\boldsymbol{\gamma}(\boldsymbol{H}))$ where $\boldsymbol{B}$ is the magnetic induction. To link the local field $\boldsymbol{H}$ with the applied one $\boldsymbol{H}^\infty$, we can utilize a recent result, which is valid for an arbitrary nonlinear and anisotropic ellipsoidal particle embedded in a linear but anisotropic matrix [52]. We consider an ellipsoidal inhomogeneity (having semi-axes a_1, a_2 and a_3) described by the (magnetic field dependent) permeability tensor $\hat{\mu}_2 = \hat{\mu}_2(\boldsymbol{H})$ embedded in a linear matrix with permeability tensor $\hat{\mu}_1$. In these conditions, we have the implicit equation:

$$\boldsymbol{H} = \left\{\hat{I} - \hat{S}_m\left[\hat{I} - \hat{\mu}_1^{-1}\hat{\mu}_2(\boldsymbol{H})\right]\right\}^{-1}\boldsymbol{H}^\infty, \tag{2}$$

where $\hat{S}_m$ is the magnetic Eshelby tensor [52]. By using the definition of the constitutive equation of the particle $\boldsymbol{B} = \hat{\mu}_2(\boldsymbol{H})\boldsymbol{H} = \mu_0(\boldsymbol{H}+\boldsymbol{M})$, we can rewrite equation (2) in a different form:

$$\begin{aligned}\boldsymbol{H} &= \left[\hat{I} - \hat{S}_m\left(\hat{I} - \hat{\mu}_1^{-1}\mu_0\right)\right]^{-1}\left[\boldsymbol{H}^{\infty} - \hat{S}_m\hat{\mu}_1^{-1}\mu_0 M_s\boldsymbol{\gamma}\right] \\ &= \hat{A}\boldsymbol{H}^{\infty} + \hat{N}\boldsymbol{\gamma}, \end{aligned} \tag{3}$$

where the tensor $\hat{N}$ is symmetric. The local magnetic field is now written in terms of the remotely applied magnetic field and of the internal magnetization orientation.

The minimization of equation (1) is constrained by the condition $\boldsymbol{\gamma}\times\boldsymbol{\gamma} = 1$. So, we can apply the Lagrange method leading to an unconstrained minimization of the function $\mathcal{L}(\boldsymbol{\gamma},\lambda) = w(\boldsymbol{\gamma}) - \lambda(\boldsymbol{\gamma}\times\boldsymbol{\gamma} - 1)$ (λ is the so-called Lagrange multiplier). Therefore, we consider the equations $\partial\mathcal{L}/\partial\gamma_i = 0$ (for $i = 1,2,3$) and $\partial\mathcal{L}/\partial\lambda = 0$. We straightforwardly obtain a system composed of $2\lambda\gamma_i = -\mu_0 M_s H_i$, $\boldsymbol{\gamma}\times\boldsymbol{\gamma} = 1$ and $\boldsymbol{H} = \hat{A}\boldsymbol{H}^{\infty} + \hat{N}\boldsymbol{\gamma}$. By combining these equations and using the symmetry of $\hat{N}$ we obtain:

$$2\lambda\gamma_i = -\mu_0 M_s\frac{\partial\left(\boldsymbol{\gamma}\hat{A}\boldsymbol{H}^{\infty}\right)}{\partial\gamma_i} - \frac{1}{2}\mu_0 M_s\frac{\partial\left(\boldsymbol{\gamma}\hat{N}\boldsymbol{\gamma}\right)}{\partial\gamma_i}. \tag{4}$$

The previous expression (with $\boldsymbol{\gamma}\times\boldsymbol{\gamma} = 1$) corresponds to a constrained minimization of a new energy function

$$\tilde{w} = -\mu_0 M_s\boldsymbol{\gamma}\hat{A}\boldsymbol{H}^{\infty} - \frac{1}{2}\mu_0 M_s\boldsymbol{\gamma}\hat{N}\boldsymbol{\gamma}, \tag{5}$$

which is advantageous since its minimization leads directly to the final magnetization orientation in terms of the externally applied field.

3 Brief outline of the statistical mechanics of magnetization

The magnetic system is assumed to be monodomain and, therefore, all spins behave collectively. The dynamics of the magnetization direction $\boldsymbol{\gamma}$ is, therefore, described by the LLG equation [44–47]:

$$\frac{\mathrm{d}\boldsymbol{\gamma}}{\mathrm{d}t} = -\frac{\mathcal{G}}{M_s(1+\alpha^2)}\left[\boldsymbol{\gamma}\wedge\frac{\partial\tilde{w}}{\partial\boldsymbol{\gamma}} - \alpha\boldsymbol{\gamma}\wedge\left(\boldsymbol{\gamma}\wedge\frac{\partial\tilde{w}}{\partial\boldsymbol{\gamma}}\right)\right], \tag{6}$$

where $\mathcal{G}$ is the gyromagnetic ratio, α is the Gilbert damping parameter and $\frac{\partial\tilde{w}}{\partial\boldsymbol{\gamma}}$ represents the effective field applied to the magnetic dipole. Here, $\tilde{w}$ is the generalized energy function defined in equation (5). The problem of introducing the damping process in the evolution equation of the magnetization dynamic is a topic largely discussed in literature [53–57]. The previous LLG equation has been generalized by Brown to implement the non-equilibrium statistical mechanics: he assumed that the effects of the temperature are mimicked by an addictive random field [48–51]. It means that he substituted in equation (6) the term $\frac{\partial\tilde{w}}{\partial\boldsymbol{\gamma}}$ with $\frac{\partial\tilde{w}}{\partial\boldsymbol{\gamma}} + \mathcal{D}\boldsymbol{n}$, where $\boldsymbol{n}$ is a stochastic process with three properties: $\langle\boldsymbol{n}(t)\rangle = 0$, $\langle n_i(t)n_j(\tau)\rangle = 2\delta_{ij}\delta(t-\tau)$, and it is Gaussian. It is well known that the combination of dissipation and fluctuation is able to describe the transient state leading to the equilibrium thermodynamics [36,37]. It is a general concept valid both in classical mechanics [58,59] and in quantum one [60,61]. We remark that a refined technique for approaching the random rotation of classical spins is based on the oscillator-bath environment [62]. However, the Brown hypothesis leads to a stochastic differential equation (SDE) [63,64]. The typical tool for studying SDEs is the Fokker-Planck methodology based on a partial differential equation describing the dynamic of the density probability of the state of the system [36]. In our case it can be written as $\rho = \rho(\varphi,\vartheta,t)$. The Fokker-Planck equation should have an asymptotic solution coherent with the equilibrium

$$\lim_{t\to\infty}\rho(\varphi,\vartheta,t) = \frac{\sin\vartheta}{\mathcal{Z}}\exp\left[-\frac{\tilde{w}(\varphi,\vartheta)v}{k_B T}\right], \tag{7}$$

where $\mathcal{Z}$ is the partition function. Here k_B is the Boltzmann constant and T is the absolute temperature. Moreover, v represents the volume of the magnetic particle ($\tilde{w}v$ is the total energy being $\tilde{w}$ the energy density). The value of the diffusion constant $\mathcal{D}$ can be found by imposing equation (7) at equilibrium: $\mathcal{D}^2 = \frac{\alpha M_s k_B T}{\mathcal{G}v}$ [48–51]. Once the value of $\mathcal{D}$ is known, we can write the Fokker-Planck equation as follows [48–51]:

$$\begin{aligned} 2\tau_N\frac{\partial\rho}{\partial t} &= \frac{v}{\alpha k_B T}\frac{1}{\sin\vartheta}\frac{\partial}{\partial\varphi}\left\{\left[\frac{\partial\tilde{w}}{\partial\vartheta} + \frac{\alpha}{\sin\vartheta}\frac{\partial\tilde{w}}{\partial\varphi}\right]\rho\right\} \\ &+ \frac{v}{\alpha k_B T}\frac{\partial}{\partial\vartheta}\left\{\left[-\frac{1}{\sin\vartheta}\frac{\partial\tilde{w}}{\partial\varphi} + \alpha\frac{\partial\tilde{w}}{\partial\vartheta}\right]\rho\right\} \\ &- \frac{\partial}{\partial\vartheta}\left\{\frac{\cos\vartheta}{\sin\vartheta}\rho\right\} + \frac{1}{\sin^2\theta}\frac{\partial^2\rho}{\partial\varphi^2} + \frac{\partial^2\rho}{\partial\vartheta^2}, \end{aligned} \tag{8}$$

where we have introduced the Néel time $\tau_N = \frac{M_s(1+\alpha^2)v}{2\alpha\mathcal{G}k_B T}$, representing the response time of a particle without external fields (see below for details). This equation has been recently used to obtain a simplified version of the Langevin system (see Refs. [42,43,65,66] for details): the Brown assumption used three random terms to add fluctuations in a system with two variables (φ and ϑ). We can consider a new version of the Langevin system where only two noise terms are considered [42,43,65,66]:

$$\begin{aligned} \dot{\varphi} &= -\frac{\mathcal{G}}{M_s(1+\alpha^2)\sin\vartheta}\left[\frac{\partial\tilde{w}}{\partial\vartheta} + \frac{\alpha}{\sin\vartheta}\frac{\partial\tilde{w}}{\partial\varphi}\right] \\ &+ \frac{1}{\sin\vartheta}\sqrt{\frac{1}{2\tau_N}}n_\phi, \\ \dot{\vartheta} &= -\frac{\mathcal{G}}{M_s(1+\alpha^2)}\left[-\frac{1}{\sin\vartheta}\frac{\partial\tilde{w}}{\partial\varphi} + \alpha\frac{\partial\tilde{w}}{\partial\vartheta}\right] \\ &+ \frac{1}{2\tau_N}\frac{\cos\vartheta}{\sin\vartheta} + \sqrt{\frac{1}{2\tau_N}}n_\theta. \end{aligned} \tag{9}$$

If the noises have the standard properties $\langle n_\phi(t)\rangle = 0$, $\langle n_\theta(t)\rangle = 0$, $\langle n_\phi(t)n_\theta(\tau)\rangle = 0$, $\langle n_\phi(t)n_\phi(\tau)\rangle = 2\delta(t-\tau)$,

$\langle n_\theta(t) n_\theta(\tau)\rangle = 2\delta(t-\tau)$ and they are Gaussian, it is possible to prove that the Fokker-Planck equation established starting form equation (9) is exactly coincident to equation (8). From the theoretical point of view equation (9) is more coherent since the SDE lives completely on the spherical surface without the need for a three-dimensional embedding (it represents the covariant formulation of the SDE on the spherical manifold) [65,66]. Moreover, from the computational point of view equation (9) is convenient since only two random numbers must be generated at any time step.

To conclude, to study the thermal effects on the magnetization dynamics we can adopt one of the three following computational methodologies. First, we can take into consideration the Fokker-Planck equation and we can search its solution through the finite difference (or element) method [67–69]. As second approach, it is possible to develop the density probability in a series of harmonic functions and to analyse the dynamics of the related coefficients. The kinetic equation for these coefficients has been obtained [70–72] and it has been largely used for determining the relaxation time of the Fokker-Planck operator [73–76]. Finally, the third approach consists in numerically solving the Langevin equation and in calculating the relevant average values through the Monte Carlo method [77]. In the following, we adopt this approach with a standard integration scheme (see Ref. [77] for details).

Langevin equations for isotropic ellipsoidal particles

If we consider isotropic ellipsoidal particles, equation (5) can be strongly simplified: we have $\hat{\mu}_1 = \mu_1 \hat{I}$ where μ_1 is the scalar permeability and $\hat{I}$ is the identity tensor. Therefore, we obtain a simpler version of the magnetic Eshelby tensor $\hat{S}_m = \mathrm{diag}\,(L_1, L_2, L_3)$ where the L_i's are the so-called depolarization factors [78]. Moreover, also the tensors $\hat{A}$ and $\hat{N}$ become diagonal with the following simplified forms:

$$A_{ij} = \frac{\mu_1 \delta_{ij}}{(1-L_i)\,\mu_1 + L_i \mu_0}, \quad N_{ij} = \frac{-L_i \mu_0 M_s \delta_{ij}}{(1-L_i)\,\mu_1 + L_i \mu_0}. \tag{10}$$

If we consider an ellipsoid of revolution with $L_1 = L_2 = L$ and $L_3 = 1 - 2L$ and a magnetic field H^∞ aligned with the z-axis, we have from equation (5):

$$\tilde{w} = -\frac{2\alpha k_B T \tau_N}{v}\left(\omega_0 \cos\vartheta + \frac{\delta}{2}\sin^2\vartheta\right) + \text{const.},$$

where we defined the parameters

$$\omega_0 = \frac{\mathcal{G}\mu_0\mu_1 H^\infty}{(1+\alpha^2)[2L\mu_1 + (1-2L)\mu_0]},$$

$$\delta = \frac{\mathcal{G}\mu_0^2\mu_1(1-3L)M_s}{(1+\alpha^2)[(1-L)\mu_1 + L\mu_0][2L\mu_1 + (1-2L)\mu_0]}. \tag{11}$$

If there is no contrast between the magnetic permeabilities, $\mu_1 = \mu_0$, we have the simplified expressions:

$$\omega_0 = \frac{\mathcal{G}\mu_0 H^\infty}{1+\alpha^2} \quad \text{and} \quad \delta = \frac{\mathcal{G}\mu_0(1-3L)M_s}{1+\alpha^2}. \tag{12}$$

We remark that $\delta \neq 0$ only for non-spherical particles: the ellipsoidal shape produces a geometrical anisotropy in the system, effectively described by this parameter.

For our purpose, we can substitute equation (11) in equation (9) and we obtain the following Langevin LLG equations for an ellipsoid of revolution:

$$\begin{aligned}
\dot{\varphi} &= \delta\cos\vartheta - \omega_0 + \frac{1}{\sin\vartheta}\sqrt{\frac{1}{2\tau_N}}n_\phi, \\
\dot{\vartheta} &= \alpha\sin\vartheta(\delta\cos\vartheta - \omega_0) + \frac{1}{2\tau_N}\frac{\cos\vartheta}{\sin\vartheta} + \sqrt{\frac{1}{2\tau_N}}n_\theta.
\end{aligned} \tag{13}$$

Some particular cases will be studied below. To do this we will adopt the parameters: $\mu_0 = \mu_1 = 4\pi \times 10^{-7}$ N/A^2 (particle in air), $M_s = 64 \times 10^4$ A/m (saturation magnetization for Terfenol), $\mathcal{G} = 1.76 \times 10^{11}$ rad s^{-1}T^{-1} ($\mathcal{G} = g\mu_B/\hbar$ where $g = 2$ is the Landé factor and μ_B is the Bohr magneton), $\alpha = 0.3$ (typical for ferrimagnetic rare earth-transition metal) and $v = 9.4 \times 10^{-23}$ m^3 (for a radius particle of about 28 nm).

4 Random walk on a spherical surface

We consider the simplest case concerning a spherical particle without magnetic field applied to the structure: in this situation the magnetization follows a random walk on the unit sphere. This problem is widely dealt with in mathematical literature and it has been approached with several different techniques [66,79,80]. From our point of view, the Langevin equation can be obtained from equation (9) by letting $\tilde{w} = 0$:

$$\begin{aligned}
\dot{\varphi} &= \frac{1}{\sin\vartheta}\sqrt{\frac{1}{2\tau_N}}n_\phi, \\
\dot{\vartheta} &= \frac{1}{2\tau_N}\frac{\cos\vartheta}{\sin\vartheta} + \sqrt{\frac{1}{2\tau_N}}n_\theta.
\end{aligned} \tag{14}$$

Hence, as above said, only the coefficient τ_N controls the dynamics in this case. On the other hand, starting from the Fokker-Planck equation, we can find the dynamics of some expected values of the random variables φ and ϑ. So, we can compare these analytical solutions with the numerical ones obtained from equation (14). A standard technique for solving this Fokker-Planck equation, largely discussed in Section 7.3 of reference [81], yields the first order and the second order expectation values of the components of $\boldsymbol{\gamma}$:

$$\langle\gamma_i\rangle = \gamma_{i0}\mathrm{e}^{-\frac{t}{\tau_N}}, \tag{15}$$

$$\langle\gamma_i\gamma_j\rangle = \gamma_{i0}\gamma_{j0}\mathrm{e}^{-3\frac{t}{\tau_N}} + \frac{1}{3}\delta_{ij}\left(1 - \mathrm{e}^{-3\frac{t}{\tau_N}}\right), \tag{16}$$

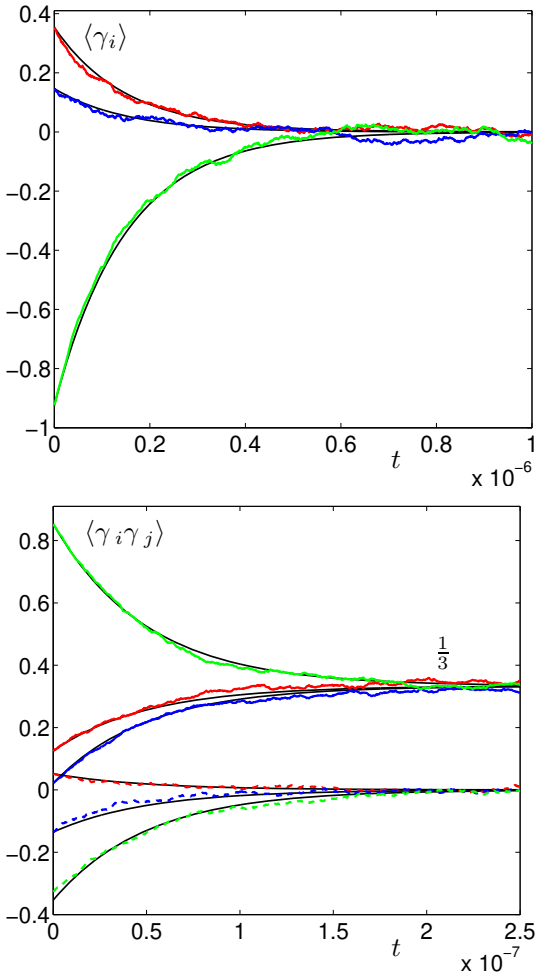

Fig. 2. Dynamics of $\boldsymbol{\gamma}$ for a spherical particle without external field. Top panel: red, blue and green lines correspond to $\langle\gamma_x\rangle$, $\langle\gamma_y\rangle$ and $\langle\gamma_z\rangle$, respectively, obtained with the Monte Carlo method. Bottom panel: red, blue and green continuous lines correspond to the averages of γ_x^2, γ_y^2 and γ_z^2 while red, blue and green dashed lines correspond to the averages of $\gamma_x\gamma_y$, $\gamma_y\gamma_z$ and $\gamma_z\gamma_x$. In both cases, the black lines correspond to equations (15) and (16).

where $\boldsymbol{\gamma}_0$ is the initial direction coherent with the angles φ_0 and ϑ_0. These expressions suggest the meaning of the Néel time τ_N: it is the time constant governing the approaching to zero of the average value of $\boldsymbol{\gamma}$ starting from a definite state and evolving without any applied field. The density probability converges, asymptotically for large time, to a uniform distribution over the spherical surface. It is important to remark that, while the norm of $\boldsymbol{\gamma}$ is unitary instantaneously, its average value can be less than one for evident statistical reasons. In the present case, the average value converges to zero because of the isotropic statistical distribution of $\boldsymbol{\gamma}$ for large time. In Figure 2, we have compared the exact solutions given in equations (15) and (16) with the numerical integration of equation (14). We adopted $\varphi_0 = \pi/8$, $\vartheta_0 = 7\pi/8$, $\tau_N = 1.5\times10^{-7}$ s (at $T = 300$ K). Moreover, we integrated equation (14) with a time step $\delta t = 1.5\times10^{-10}$ s and the final curves have been obtained by averaging $M = 1000$ independent trajectories through the Monte Carlo method.

5 Spherical particle under magnetic field

We consider now a spherical particle subjected to a uniform magnetic field: we have now $\omega_0 \neq 0$ and, therefore, the Langevin system assumes the form:

$$\dot{\varphi} = -\omega_0 + \frac{1}{\sin\vartheta}\sqrt{\frac{1}{2\tau_N}}n_\phi, \tag{17}$$
$$\dot{\vartheta} = -\omega_0\alpha\sin\vartheta + \frac{1}{2\tau_N}\frac{\cos\vartheta}{\sin\vartheta} + \sqrt{\frac{1}{2\tau_N}}n_\theta.$$

Without thermal effects ($T = 0$ K or $\tau_N \to \infty$) it is possible to obtain the closed form solution of equation (17) corresponding to the initial conditions $\varphi(0) = \varphi_0$, $\vartheta(0) = \vartheta_0$; the result is given by:

$$\boldsymbol{\gamma} = \begin{pmatrix} \dfrac{\cos(\omega_0 t - \varphi_0)\sin\vartheta_0}{\cosh(\omega_0\alpha t) + \cos\vartheta_0\sinh(\omega_0\alpha t)} \\ \dfrac{-\sin(\omega_0 t - \varphi_0)\sin\vartheta_0}{\cosh(\omega_0\alpha t) + \cos\vartheta_0\sinh(\omega_0\alpha t)} \\ \dfrac{\sinh(\omega_0\alpha t) + \cos\vartheta_0\cosh(\omega_0\alpha t)}{\cosh(\omega_0\alpha t) + \cos\vartheta_0\sinh(\omega_0\alpha t)} \end{pmatrix}. \tag{18}$$

This solution is a particular case of a more general result obtained in reference [82]. If $\varphi(0) = 0$, $\vartheta(0) = \pi/2$, we obtain the simpler result:

$$\boldsymbol{\gamma} = \left(\frac{\cos(\omega_0 t)}{\cosh(\omega_0\alpha t)}, -\frac{\sin(\omega_0 t)}{\cosh(\omega_0\alpha t)}, \frac{\sinh(\omega_0\alpha t)}{\cosh(\omega_0\alpha t)}\right), \tag{19}$$

which represents the classical damped precession motion of the magnetization direction towards the perfect alignment with the applied magnetic field (along the z-axis in the present case). When the temperature is taken into account it is difficult to obtain closed form expressions describing the dynamics of the system (see Sect. 7.5 of Ref. [37] for details). However, we can analytically study the asymptotic thermodynamic equilibrium. In fact, from equation (7) we easily obtain the Gibbs distribution describing the probability density of the angles at equilibrium

$$\rho_{eq}(\varphi,\vartheta) = \frac{\alpha\tau_N\omega_0\sin\vartheta}{2\pi\sinh(2\alpha\tau_N\omega_0)}\mathrm{e}^{2\alpha\tau_N\omega_0\cos\vartheta}. \tag{20}$$

Of course, it depends only on the angle ϑ for the axial symmetry of the system. The knowledge of such a distribution allow us to determine the average values of the components of $\boldsymbol{\gamma}$:

$$\langle\gamma_x\rangle = \langle\gamma_y\rangle = 0, \tag{21}$$
$$\langle\gamma_z\rangle = \langle\cos\vartheta\rangle = \mathcal{L}(2\alpha\tau_N\omega_0), \tag{22}$$

where $\mathcal{L}(x) = \coth x - 1/x$ is the classical Langevin function. The value of $\langle\gamma_z\rangle$ approaches 1 at $T = 0$ K and

it is a decreasing function with the temperature: in fact, the area around the north pole spanned by the magnetization vector is increasing with temperature, lowering at the same time the net magnetization along the z-axis. In the context of the particles suspensions, equation (22) is useful to explain the superparamagnetic behavior observed under the dilute conditions [1–4]. This result is also in perfect agreement with the theory of the magnetic polarization (for paramagnetic materials) or the electric polarization (when the orientation of polar molecules takes place) [83,84]. There is also a strong mathematical analogy with the problem of determining the elastic response of flexible polymer under external forces (in this case, each bond between two adjacent monomers behaves like a dipole under an external field) [85,86]. Moreover, we can also calculate the second order expectation values, eventually obtaining the following results:

$$\left\langle \gamma_x^2 \right\rangle = \left\langle \gamma_y^2 \right\rangle = \frac{\mathcal{L}(2\alpha\tau_N\omega_0)}{2\alpha\tau_N\omega_0}, \tag{23}$$

$$\left\langle \gamma_z^2 \right\rangle = 1 - \frac{\mathcal{L}(2\alpha\tau_N\omega_0)}{\alpha\tau_N\omega_0}, \tag{24}$$

$$\left\langle \gamma_x\gamma_y \right\rangle = \left\langle \gamma_y\gamma_z \right\rangle = \left\langle \gamma_z\gamma_x \right\rangle = 0. \tag{25}$$

In Figure 3, one can find an example of numerical solution of equation (17) for a particle with $\varphi(0) = \pi/8$, $\vartheta(0) = 7\pi/8$, $\omega_0 = 10^8$ s^{-1}, $\tau_N = 1.5 \times 10^{-7}$ s (at $T = 300$ K) and $\delta t = 1.5 \times 10^{-10}$ s (with $M = 1000$ Monte Carlo trials). In the top panel, we note that while $\langle \gamma_z \rangle$ converges monotonically to the asymptotic value given by equation (22), $\langle \gamma_x \rangle$ and $\langle \gamma_y \rangle$ exhibit a series of damped oscillations, representing rotations of the magnetization around the direction of the applied field (precession). On the other hand, in the bottom panel the behavior of the second order expectation values is shown. The limiting values given in equations (23)−(25) are in agreement with simulations.

Starting with equation (20), we can also determine the expression of the variance of the z-component of $\boldsymbol{\gamma}$, which is useful for the interpretation of the following numerical results:

$$\sigma_z^2 = 1 - \frac{\mathcal{L}(2\alpha\tau_N\omega_0)}{\alpha\tau_N\omega_0} - \left[\mathcal{L}(2\alpha\tau_N\omega_0)\right]^2. \tag{26}$$

We can evaluate the thermal effects on the orientation dynamics: in Figure 4 one can find the behavior of $\langle \gamma_z \rangle$, $\langle \gamma_z^2 \rangle$ and σ_z^2 for different values of the temperature. In these numerical calculations, we assumed $\varphi(0) = 0$, $\vartheta(0) = \pi/2$, $\omega_0 = 10^8$ s^{-1}, a time step $\delta t = 10^{-10}$ s and the final curves have been obtained by averaging $M = 5000$ independent trajectories (Monte Carlo method). We adopted 15 different values of the temperature equispaced between 5 K and 2105 K (with an incremental step of 150 K). These very high values may be non-physical, but they are useful to test the numerical schemes and to understand the behavior of the system. The first curves have been obtained at nearly zero temperature and they are indeed in perfect agreement with equation (19), representing a deterministic result. Moreover, the asymptotic behavior of all curves

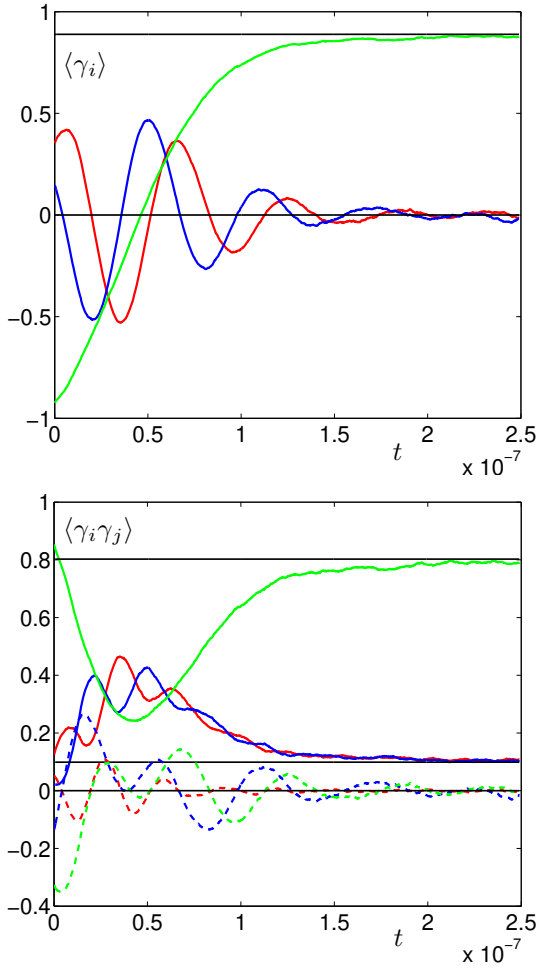

Fig. 3. Dynamics of $\boldsymbol{\gamma}$ for a spherical particle under externally applied magnetic field. Top panel: red, blue and green lines correspond to $\langle \gamma_x \rangle$, $\langle \gamma_y \rangle$ and $\langle \gamma_z \rangle$, respectively, obtained with the Monte Carlo method. Bottom panel: red, blue and green continuous lines correspond to the averages of γ_x^2, γ_y^2 and γ_z^2 while red, blue and green dashed lines correspond to the averages of $\gamma_x\gamma_y$, $\gamma_y\gamma_z$ and $\gamma_z\gamma_x$. In both cases, the black lines correspond to equations (21)−(25).

correspond perfectly to equations (22)−(26), as expected. We remark that $\langle \gamma_z \rangle$ and $\langle \gamma_z^2 \rangle$ are decreasing function of the temperature, while σ_z^2 is increasing, measuring effectively the intensity of the fluctuations.

It is important to remark that the velocity of convergence towards the thermodynamic equilibrium depends on the temperature. Therefore, we can introduce a convergence time t_m (between $\vartheta = \pi/2$ and $\vartheta = 0$) and investigate its dependence on T. The time t_m is defined as the first instant of time when the condition $|\langle \gamma_z \rangle (t_m) - \langle \gamma_z \rangle (\infty)| < \epsilon_\gamma$ is satisfied (here, we used $\epsilon_\gamma = 3/100$). The behavior of t_m versus T is reported in Figure 5. For any temperature we have generated $n = 100$ averaged trajectories (for each of them we used $\delta t = 10^{-10}$ s and we calculated the mean value over $M = 5000$ samples), corresponding to the circles in Figure 5 (top panel). On the other hand, the squares represent the average t_m over

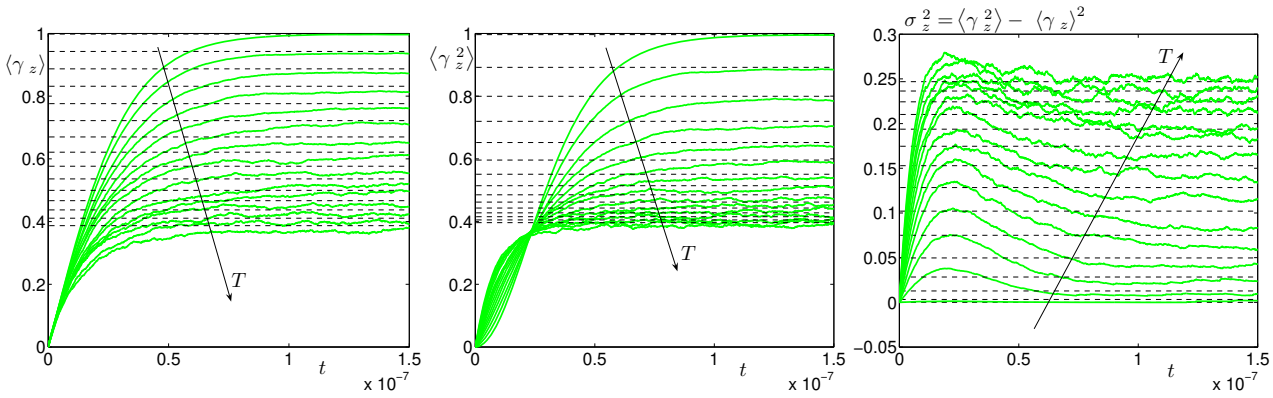

Fig. 4. Time behavior of $\langle \gamma_z \rangle$ (left panel), $\langle \gamma_z^2 \rangle$ (central panel) and σ_z^2 (right panel) for different values of the temperature. Black dashed lines in each plot correspond to the asymptotic regime (equilibrium thermodynamics) given by equations (22)−(26), respectively.

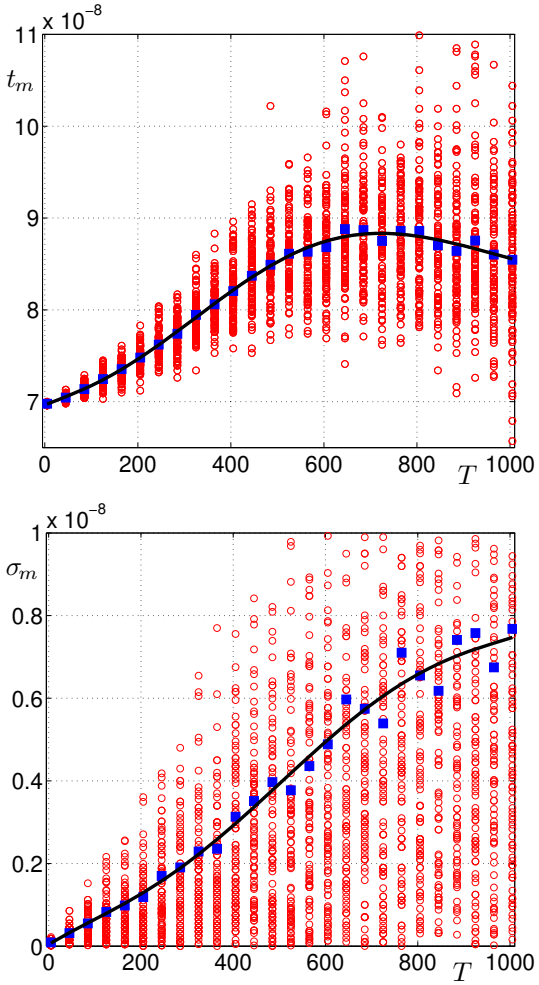

Fig. 5. Convergence time t_m (top) and its standard deviation σ_m (bottom) for a spherical particle under a magnetic field applied along a given direction.

the $n = 100$ different values t_i $(i = 1, \ldots, 100)$. In the bottom panel, we report the standard deviation σ_m of the quantity t_m. It is defined through the relation $\sigma_m^2 = \sum_{i=1}^{n}(t_i - t_m)^2/(n-1)$, where $n = 100$; here the circles represent the deviations $|t_i - t_m|$ $(i = 1, \ldots, 100)$. In the top panel of Figure 5, we note a non-monotone behavior of t_m versus T. The first increasing part of the curve means that the fluctuations introduced by the temperature slow down the convergence to the thermodynamic equilibrium; nevertheless, the trend becomes decreasing for high temperatures since the asymptotic value of $\langle \gamma_z \rangle$ (see Fig. 4) is much lower and, therefore, it can be rapidly reached in spite of thermal fluctuations.

6 Ellipsoidal particle without magnetic field

We study the free motion of the magnetization within an ellipsoidal particle. In particular, we are interested in understanding the different behavior of prolate and oblate particles. The dynamics of the system is described by equation (13) with $\omega_0 = 0$ (i.e. $H^\infty = 0$):

$$\begin{aligned} \dot{\varphi} &= \delta \cos\vartheta + \frac{1}{\sin\vartheta}\sqrt{\frac{1}{2\tau_N}}n_\phi, \\ \dot{\vartheta} &= \alpha\delta \sin\vartheta\cos\vartheta + \frac{1}{2\tau_N}\frac{\cos\vartheta}{\sin\vartheta} + \sqrt{\frac{1}{2\tau_N}}n_\theta. \end{aligned} \tag{27}$$

In order to understand the effects of the non-sphericity, at the beginning we consider the system at $T = 0$ K and we obtain, after some long but straightforward calculations the solution for an arbitrary φ_0 and for $\vartheta_0 \in (0, \pi/2)$:

$$\varphi = \varphi_0 + \frac{1}{2\alpha}\ln\left\{\frac{\sqrt{1+\tan^2\vartheta_0}+1}{\sqrt{1+\tan^2\vartheta_0}-1} \times \frac{\sqrt{1+\tan^2\vartheta_0 e^{2\alpha\delta t}}-1}{\sqrt{1+\tan^2\vartheta_0 e^{2\alpha\delta t}}+1}\right\}, \tag{28}$$

$$\cos\vartheta = \frac{1}{\sqrt{1+\tan^2\vartheta_0 e^{2\alpha\delta t}}}, \tag{29}$$

$$\sin\vartheta = \frac{\tan\vartheta_0 e^{\alpha\delta t}}{\sqrt{1+\tan^2\vartheta_0 e^{2\alpha\delta t}}}. \tag{30}$$

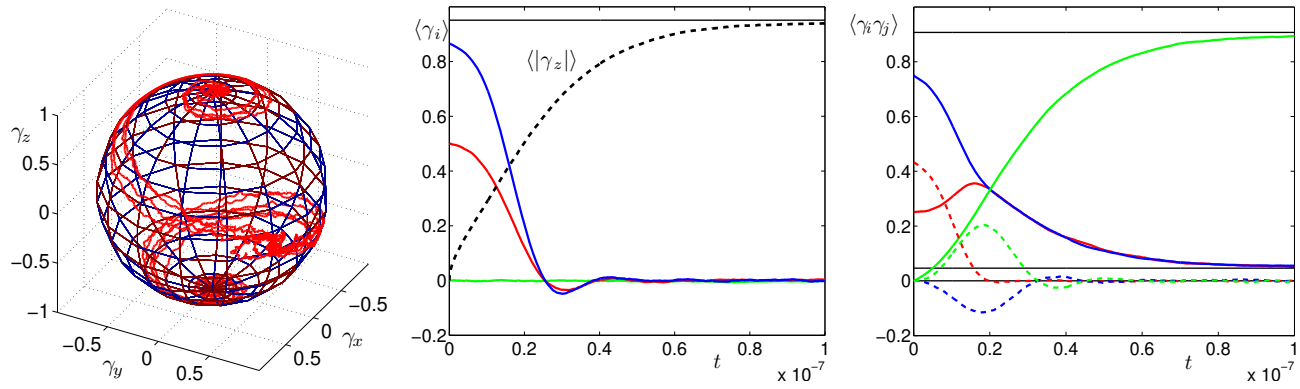

Fig. 6. Numerical results for a prolate particle without applied fields. First panel: examples of trajectories starting from $\varphi(0) = \pi/3$ and $\vartheta(0) = \pi/2$. Central panel: average values of γ_x (red curve), γ_y (blue curve), γ_z (green curve) and $|\gamma_z|$ (black dashed curve). The black solid line corresponds to the asymptotic value given in equation (39). Third panel: red, blue and green solid lines correspond to the averages of γ_x^2, γ_y^2 and γ_z^2 while red, blue and green dashed lines correspond to the averages of $\gamma_x\gamma_y$, $\gamma_y\gamma_z$ and $\gamma_z\gamma_x$. Black lines correspond to equations (36)−(38).

Now, we may observe that δ is proportional to $1-3L$ and therefore we have: (i) $\delta < 0$ for prolate particles ($L > 1/3$) and (ii) $\delta > 0$ for oblate particles ($L < 1/3$). The important result is that, for an arbitrary initial condition we have: (i) a reorientation of the magnetization along the z-axis (in the positive direction if $0 < \vartheta_0 < \pi/2$ and in the negative direction if $\pi/2 < \vartheta_0 < \pi$) for prolate particles ($\cos\vartheta \to \pm 1$ if $t \to \infty$) and (ii) a reorientation on the plane xy for oblate particles ($\cos\vartheta \to 0$ if $t \to \infty$). In this latter case ($\delta > 0$), there exists an asymptotic value of the angle φ given by the following expression:

$$\lim_{t\to\infty} \varphi = \varphi_0 + \frac{1}{2\alpha} \ln \frac{\sqrt{1+\tan^2\vartheta_0}+1}{\sqrt{1+\tan^2\vartheta_0}-1}, \qquad (31)$$

corresponding to a finite number of precession rotations.

When the system is embedded in a thermal bath at temperature T we can analyse the thermodynamic equilibrium through equation (7): after some calculations we obtain:

$$\rho_{eq}(\varphi,\vartheta) = \frac{\sin\vartheta \mathrm{e}^{\alpha\tau_N\delta\sin^2\vartheta}}{2\pi\sqrt{\frac{\pi}{\alpha\tau_N\delta}}\ \mathrm{e}^{\alpha\tau_N\delta}\mathrm{erf}\left(\sqrt{\alpha\tau_N\delta}\right)} \qquad (32)$$

if $\delta > 0$ (oblate particle) and

$$\rho_{eq}(\varphi,\vartheta) = \frac{\sin\vartheta \mathrm{e}^{-\alpha\tau_N\varepsilon\sin^2\vartheta}}{2\pi\sqrt{\frac{\pi}{\alpha\tau_N\varepsilon}}\ \mathrm{e}^{-\alpha\tau_N\varepsilon}\mathrm{erfi}\left(\sqrt{\alpha\tau_N\varepsilon}\right)} \qquad (33)$$

if $\delta = -\epsilon < 0$ (prolate particle), where we used the functions $\mathrm{erf}(z)$ and $\mathrm{erfi}(z)$ defined below [87]

$$\mathrm{erf}(z) = \frac{2}{\sqrt{\pi}}\int_0^z \mathrm{e}^{-t^2}dt, \qquad (34)$$

$$\mathrm{erfi}(z) = \frac{2}{\sqrt{\pi}}\int_0^z \mathrm{e}^{t^2}dt. \qquad (35)$$

The obtained Gibbs distributions, equations (32) and (33), will be used to determine some relevant expectation values, useful to compare the theory with numerical results for both prolate and oblate particles.

6.1 Prolate particle: an axial geometrical anisotropy

In Figure 6, we can observe an example of numerical solution of equation (27). We adopted the parameters $\tau_N = 1.5\times10^{-7}$ s (at $T = 300$ K) and $\delta = -2.58\times10^8$ s^{-1}. In the first panel, we can find a series of trajectories starting from $\varphi(0) = \pi/3$ and $\vartheta(0) = \pi/2$: since $\vartheta(0) = \pi/2$ corresponds to an unstable position each trajectory converges with the same probability either towards the north or the south pole of the sphere. In the central panel, we report the average values $\langle\gamma_x\rangle$, $\langle\gamma_y\rangle$ and $\langle\gamma_z\rangle$, converging asymptotically to zero, and in the last panel, the second order expectation quantities converging to the following values (calculated by means of Eq. (33)):

$$\langle\gamma_x^2\rangle = \langle\gamma_y^2\rangle = \frac{1-\langle\gamma_z^2\rangle}{2}, \qquad (36)$$

$$\langle\gamma_z^2\rangle = \frac{\mathrm{e}^{\alpha\tau_N\varepsilon}}{\sqrt{\pi\alpha\tau_N\varepsilon}\ \mathrm{erfi}\left(\sqrt{\alpha\tau_N\varepsilon}\right)} - \frac{1}{2\alpha\tau_N\varepsilon}, \qquad (37)$$

$$\langle\gamma_x\gamma_y\rangle = \langle\gamma_y\gamma_z\rangle = \langle\gamma_z\gamma_x\rangle = 0. \qquad (38)$$

Since $\langle\gamma_z\rangle \to 0$ (as $t \to \infty$) for symmetry, we can introduce $\langle|\gamma_z|\rangle$ (dashed line in Fig. 6, central panel), which converges to the asymptotic value

$$\langle|\gamma_z|\rangle = \frac{\mathrm{e}^{\alpha\tau_N\varepsilon}-1}{\sqrt{\pi\alpha\tau_N\varepsilon}\ \mathrm{erfi}\left(\sqrt{\alpha\tau_N\varepsilon}\right)}. \qquad (39)$$

In Figure 7 (first panel), we can observe the behavior of such a quantity $\langle|\gamma_z|\rangle$ for different temperatures. We can define t_m as the convergence time of $\langle|\gamma_z|\rangle$ to its its asymptotic value given in equation (39). In the central panel of Figure 7, we report the behavior of t_m versus T (obtained with a confidence parameter $\epsilon_\gamma = 2/100$) and in the third one the corresponding standard deviation (defined as above). The trajectories of the magnetization start from $\vartheta = \pi/2$ that is an unstable equilibrium point for the prolate particle and, therefore, if $T \to 0$ we have $t_m \to \infty$. This asymptotic trend is evident in the second panel of

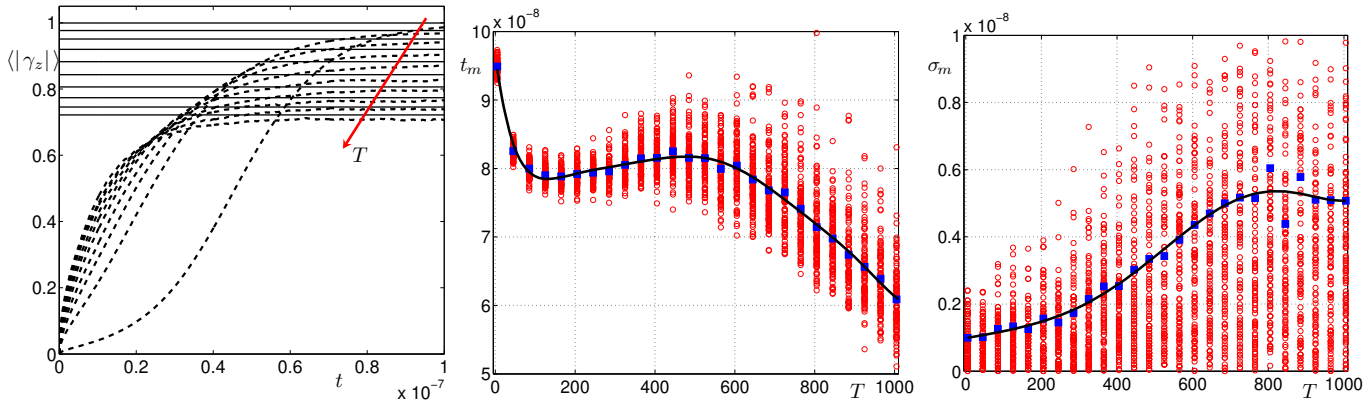

Fig. 7. Temperature effects on the reorientation process for a prolate particle. First panel: behavior of $\langle|\gamma_z|\rangle$ for different temperatures (ten values from 5 K to 1355 K with a step of 150 K). Second panel: convergence time t_m versus T. Third panel: standard deviation σ_m of the convergence time versus T.

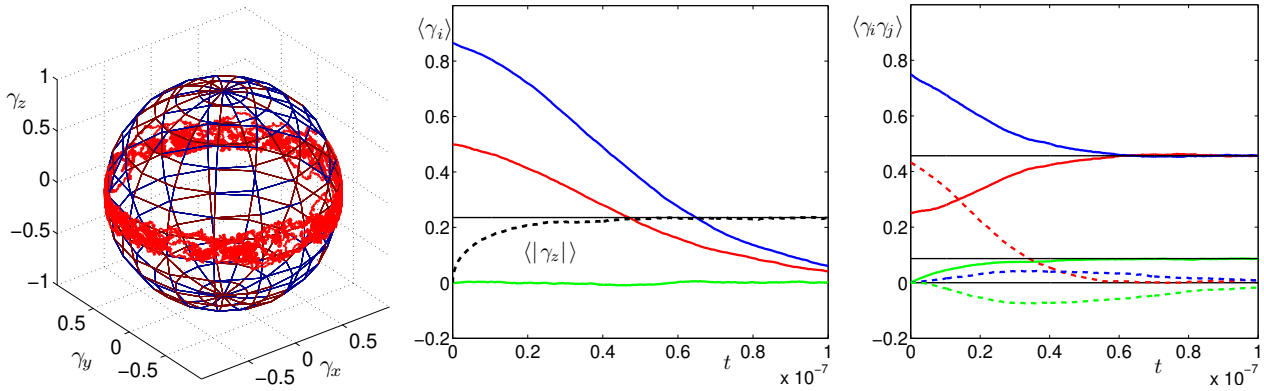

Fig. 8. Numerical results for an oblate particle without applied fields. First panel: examples of trajectories starting from $\varphi(0) = \pi/3$ and $\vartheta(0) = \pi/2$. Central panel: average values of γ_x (red curve), γ_y (blue curve), γ_z (green curve) and $|\gamma_z|$ (black dashed curve). The black solid line corresponds to the asymptotic value given in equation (43). Third panel: red, blue and green solid lines correspond to the averages of γ_x^2, γ_y^2 and γ_z^2 while red, blue and green dashed lines correspond to the averages of $\gamma_x\gamma_y$, $\gamma_y\gamma_z$ and $\gamma_z\gamma_x$. Black lines correspond to equations (40)−(42).

Figure 7, where an infinitely large negative slope can be observed for $T \to 0$. The following increasing part of the curve means that fluctuations reduce the convergence velocity to the thermodynamic equilibrium at intermediate temperatures. Finally, the last decreasing trend can be explained by observing that at higher temperatures the limiting value of $\langle|\gamma_z|\rangle$ is much lower and it can be reached more quickly, in spite of thermal effects.

6.2 Oblate particle: a planar geometrical anisotropy

In Figure 8 we can observe an example of numerical solution of equation (27). We adopted the parameters $\tau_N = 1.5 \times 10^{-7}$ s (at $T = 300$ K) and $\delta = 1.3 \times 10^8$ s^{-1}. In the first panel we can find a series of trajectories starting from $\varphi(0) = \pi/3$ and $\vartheta(0) = \pi/2$: since $\vartheta(0) = \pi/2$ corresponds to a stable position each trajectory fluctuates around the equator. In the central panel, we report the average values $\langle\gamma_x\rangle$, $\langle\gamma_y\rangle$ and $\langle\gamma_z\rangle$, converging asymptotically to zero, and in the last panel the second order expectation quantities converging to the following values (calculated by means of Eq. (32)):

$$\langle\gamma_x^2\rangle = \langle\gamma_y^2\rangle = \frac{1 - \langle\gamma_z^2\rangle}{2}, \tag{40}$$

$$\langle\gamma_z^2\rangle = \frac{1}{2\alpha\tau_N\delta} - \frac{\mathrm{e}^{-\alpha\tau_N\delta}}{\sqrt{\pi\alpha\tau_N\delta}\,\mathrm{erf}\left(\sqrt{\alpha\tau_N\delta}\right)}, \tag{41}$$

$$\langle\gamma_x\gamma_y\rangle = \langle\gamma_y\gamma_z\rangle = \langle\gamma_z\gamma_x\rangle = 0. \tag{42}$$

As before, since $\langle\gamma_z\rangle \to 0$ as $t \to \infty$, we can introduce $\langle|\gamma_z|\rangle$ (dashed line in Fig. 8, central panel), which converges to the asymptotic value

$$\langle|\gamma_z|\rangle = \frac{1 - \mathrm{e}^{-\alpha\tau_N\delta}}{\sqrt{\pi\alpha\tau_N\delta}\,\mathrm{erf}\left(\sqrt{\alpha\tau_N\delta}\right)}. \tag{43}$$

In Figure 9 (first panel), we can observe the behavior of such a quantity $\langle|\gamma_z|\rangle$ for different temperatures. We can define t_m as the convergence time of $\langle|\gamma_z|\rangle$ to its asymptotic value given in equation (43). In the central panel of Figure 9, we report the behavior of t_m versus T (obtained with a confidence parameter $\epsilon_\gamma = 2/100$) and, finally, in

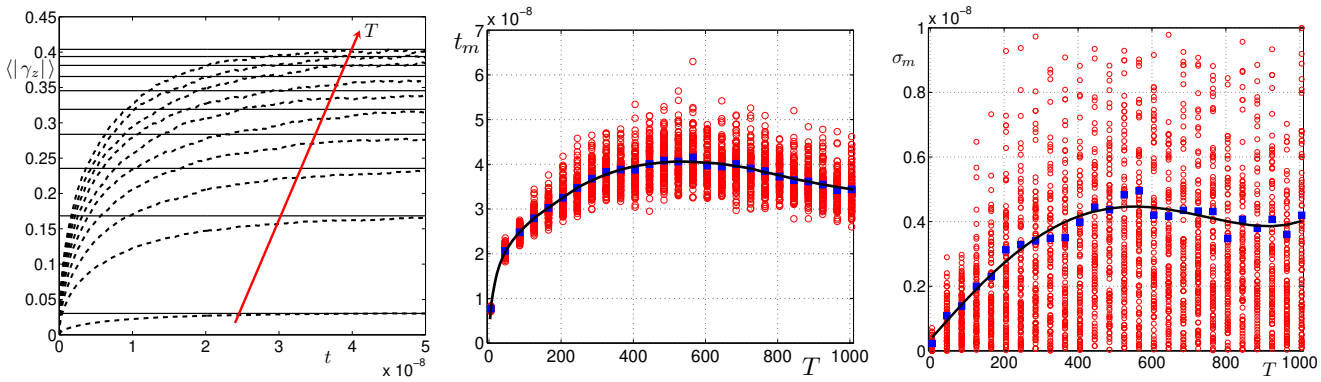

Fig. 9. Temperature effects on the reorientation process for an oblate particle. First panel: behavior of $\langle|\gamma_z|\rangle$ for different temperatures (ten values from 5 K to 1355 K with a step of 150 K). Second panel: convergence time t_m versus T. Third panel: standard deviation σ_m of the convergence time versus T.

the third one the corresponding standard deviation (defined as above). The trajectories of the magnetization start from $\vartheta = \pi/2$ that is a stable equilibrium point for the oblate particle and, therefore, if $T \to 0$ we have $t_m \to 0$. It can be seen in the second panel of Figure 9, where a large positive slope is evident for $T \to 0$. For higher temperature the curve exhibits a decreasing trend. Interestingly enough, the maximum value of t_m for oblate and prolate particles can be observed at the same temperature value.

We remark that for the configurations considered in the present paper the relaxations times (related to the Fokker-Planck operator) are known in analytical (exact or approximate) form [37]. Of course, our convergence times can be conceptually related to the relaxation times but, unfortunately, direct relationships among them are not available. As a matter of fact, the relaxation times, being related to the eigenvalues of the Fokker-Planck operator, are present in any explicit solution for the average values of the magnetization vector. However, the convergence time is strongly related to applications being the time used to reach an equilibrium position of the magnetization. For example, for an information storage system it corresponds to the switching time (used to change the state of a bit), which is an important parameter for memory devices.

7 Conclusions

In this work, we considered the effects of the temperature on the magnetization dynamics in single domain particles. In order to address the problem in a gradual manner, we initially considered the most simple cases, and at a later stage the most involved ones. We have therefore introduced a series of paradigmatic configurations of increasing complexity: (i) a spherical particle without applied fields, corresponding to a random walk on the sphere, (ii) a spherical particle subjected to an external magnetic field, and (iii) a prolate or oblate ellipsoidal particle without applied fields, corresponding to axial or planar geometrical anisotropies. In all cases, we have taken into consideration the Langevin equation describing the dynamics of the magnetization vector when the system is in contact with a thermal bath. Its numerical solution allowed us to examine the convergence time of all above-mentioned configurations in terms of the temperature. If we take into consideration a given average value concerning the magnetization dynamics, the convergence time is defined as the time used to reach the asymptotic value of this quantity with a fixed margin of error. In any case, we found non-monotone dependences versus the temperature, which correspond to a complex behavior of the considered systems. The computational outcomes concerning the non-equilibrium statistics have been supported with two kind of analytical results: (i) the dynamics at zero temperature obtained by solving in closed forms the classical LLG equation without noise, and (ii) the Gibbs probability density and some expectation values at thermodynamic equilibrium.

This work was supported by the Agence Nationale de la Recherche ANR (France) through the PNano NAMAMIS project and by the Russian Federation Ministry of Education and Sciences (Contract N. 11.519.11.3023).

References

1. R. Kaiser, G. Miskolczy, J. Appl. Phys. **41**, 1064 (1970)
2. A.L. Dantas, A.S. Carriço, N.S. Almeida, Eur. Phys. J. B **50**, 581 (2006)
3. S. Mørup, E. Tronc, Phys. Rev. Lett. **72**, 3278 (1994)
4. J. García-Otero, M. Porto, J. Rivas, A. Bunde, Phys. Rev. Lett. **84**, 167 (2000)
5. C. Kormann, H.M. Laun, H.J. Richter, Int. J. Mod. Phys. B **10**, 3167 (1996)
6. A.T. Skjeltorp, J. Appl. Phys. **57**, 3285 (1985)
7. S. Lamba, S. Annapoornia, Eur. Phys. J. B **39**, 19 (2004)
8. M. Golosovsky, Y. Saado, D. Davidov, Appl. Phys. Lett. **75**, 4168 (1999)
9. M. Shinkai, J. Biosci. Bioeng. **94**, 606 (2002)
10. I.-M. Hsing, Y. Xu, W. Zhaob, Electroanalysis **19**, 755 (2007)
11. Y.-W. Jun, J.-W. Seo, J. Cheon, Acc. Chem. Res. **41**, 179 (2008)
12. I. Safarik, M. Safarikova, BioMag. Res. Technol. **2**, 7 (2004)
13. N. Pamme, Lab on a Chip **6**, 24 (2005)

14. B. Gleich, J. Weizenecker, Nature **435**, 1214 (2005)
15. J. Weizenecker, B. Gleich, J. Rahmer, H. Dahnke, J. Borgert, Phys. Med. Biol. **54**, L1 (2009)
16. A.K. Gupta, M. Gupta, Biomaterials **26**, 3995 (2005)
17. K.J. Widder, R.M. Morris, G. Poore, D.P. Howard, A.E. Senyei, Proc. Natl. Acad. Sci. **78**, 579 (1981)
18. A. Jordan, P. Wust, R. Scholz, B. Tesch, H. Filhling, T. Mitrovics, T. Vogl, J. Cervos-Navarro, R. Felix, Int. J. Hyperthermia **12**, 705 (1996)
19. P. Moroz, S.K. Jones, B.N. Gray, Int. J. Hyperthermia **18**, 267 (2002)
20. M. Fiebig, J. Phys. D **38**, 123 (2005)
21. R. Ramesh, N.A. Spaldin, Nat. Mater. **6**, 21 (2007)
22. C.W. Nan, M.I. Bichurin, S. Dong, D. Viehland, G. Srinivasan, J. Appl. Phys. **103**, 031101 (2008)
23. N. D'Souza, J. Atulasimha, S. Bandyopadhyay, J. Phys. D **44**, 265001 (2011)
24. N.A. Pertsev, H. Kohlstedt, Nanotechnology **21**, 475202 (2010)
25. K. Roy, S. Bandyopadhyay, J. Atulasimha, Appl. Phys. Lett. **99**, 063108 (2011)
26. N. Tiercelin, Y. Dusch, V. Preobrazhensky, P. Pernod, J. Appl. Phys. **109**, 07D726 (2011)
27. N. Tiercelin, Y. Dusch, A. Klimov, S. Giordano, V. Preobrazhensky, P. Pernod, Appl. Phys. Lett. **99**, 192507 (2011)
28. S. Giordano, Y. Dusch, N. Tiercelin, P. Pernod, V. Preobrazhensky, Phys. Rev. B **85**, 155321 (2012)
29. V. Novosad, Y. Otani, A. Ohsawa, S.G. Kim, K. Fukamichi, J. Koike, K. Maruyama, O. Kitakami, Y. Shimada, J. Appl. Phys. **87**, 6400 (2000)
30. K. Roy, S. Bandyopadhyay, J. Atulasimha, Phys. Rev. B **83**, 224412 (2011)
31. K. Roy, S. Bandyopadhyay, J. Atulasimha, J. Appl. Phys. **112**, 023914 (2012)
32. J. Tejada, E.M. Chudnovsky, E. del Barco, J.M. Hernandez, T.P. Spiller, Nanotechnology **12**, 181 (2001)
33. R. Kikuchi, J. Appl. Phys. **27**, 1352 (1956)
34. G.V. Skrotskii, Sov. Phys. Usp. **27**, 977 (1984)
35. P. Hänggi, Phys. Rep. **88**, 207 (1982)
36. H. Risken, *The Fokker-Planck equation* (Springer-Verlag, Berlin, 1989)
37. W.T. Coffey, Yu. P. Kalmykov, J.P. Waldron, *The Langevin equation* (World Scientific, Singapore, 2004)
38. S.I. Denisov, Phys. Solid State **41**, 1672 (1999)
39. S.I. Denisov, K.N. Trohidou, Phys. Rev. B **64**, 184433 (2001)
40. S.I. Denisov, T.V. Lyutyy, P. Hänggi, Phys. Rev. Lett. **97**, 227202 (2006)
41. S.I. Denisov, T.V. Lyutyy, P. Hänggi, K.N. Trohidou, Phys. Rev. B **74**, 104406 (2006)
42. S.I. Denisov, K. Sakmann, P. Talkner, P. Hänggi, Phys. Rev. B **75**, 184432 (2007)
43. S.I. Denisov, A. Yu. Polyakov, T.V. Lyutyy, Phys. Rev. B **84**, 174410 (2011)
44. L. Landau, E. Lifshitz, Phys. Z. Sowjetunion **8**, 153 (1935)
45. T.L. Gilbert, Phys. Rev. **100**, 1243 (1955) (abstract only)
46. T.L. Gilbert, IEEE Trans. Mag. **40**, 3443 (2004)
47. M. Lakshmanan, Phil. Trans. R. Soc. A **369**, 1280 (2011)
48. W.F. Brown, J. Appl. Phys. **30**, S130 (1959)
49. W.F. Brown, J. Appl. Phys. **34**, 1319 (1963)
50. W.F. Brown, Phys. Rev. **130**, 1677 (1963)
51. W.F. Brown, IEEE Trans. Magn. **15**, 1196 (1979)
52. S. Giordano, P.L. Palla, J. Phys. A **41**, 415205 (2008)
53. J.C. Mallinson, IEEE Trans. Magn. **23**, 2003 (1987)
54. P. Podio-Guidugli, Eur. Phys. J. B **19**, 417 (2001)
55. G. Bertotti, I.D. Mayergoyz, C. Serpico, Physica B **306**, 102 (2001)
56. W.M. Saslow, J. Appl. Phys. **105**, 07D315 (2009)
57. J.-E. Wegrowe, M.-C. Ciornei, Am. J. Phys. **80**, 607 (2012)
58. G.E. Uhlenbeck, L.S. Ornstein, Phys. Rev. **36**, 823 (1930)
59. M.C. Wang, G.E. Uhlenbeck, Rev. Mod. Phys. **17**, 323 (1945)
60. P. Caldirola, L.A. Lugiato, Physica A **116**, 248 (1982)
61. B. Bianco, E. Moggia, S. Giordano, W. Rocchia, A. Chiabrera, Nuovo Cim. **116**, 155 (2001)
62. J.L. García-Palacios, Eur. Phys. J. B **11**, 293 (1999)
63. Z. Schuss, *Theory, Applications of Stochastic Differential Equations* (John Wiley & Sons, New York, 1980)
64. Z. Schuss, *Theory, Applications of Stochastic Processes* (Springer, New York, 2010)
65. G. Bertotti, I. Mayergoyz, C. Serpico, *Nonlinear Magnetization Dynamic in Nanosystems* (Elsevier, Oxford, 2000)
66. D.R. Fredkin, Physica B **306**, 26 (2001)
67. H. Fukushima, Y. Uesaka, Y. Nakatani, N. Hayashi, J. Magn. Magn. Mater. **242**, 1002 (2002)
68. H. Fukushima, Y. Uesaka, Y. Nakatani, N. Hayashi, IEEE Trans. Magn. **38**, 2394 (2002)
69. H. Fukushima, Y. Uesaka, Y. Nakatani, N. Hayashi, J. Magn. Magn. Mater. **272**, 745 (2004)
70. Yu.P. Kalmykov, J. Mol. Liq. **69**, 117 (1996)
71. W.T. Coffey, L.J. Geoghegan, J. Mol. Liq. **69**, 53 (1996)
72. Yu. P. Kalmykov, S.V. Titov, Phys. Rev. Lett. **82**, 2967 (1999)
73. W.T. Coffey, D.A. Garanin, H. Kachkachi, D.J. McCarthy, J. Magn. Magn. Mater. **221**, 110 (2000)
74. P.M. Déjardin, D.S.F. Crothers, W.T. Coffey, D.J. McCarthy, Phys. Rev. E **63**, 021102 (2001)
75. Yu.P. Kalmykov, W.T. Coffey, B. Ouari, S.V. Titov, J. Magn. Magn. Mater. **292**, 372 (2005)
76. B. Ouari, Yu. P. Kalmykov, J. Appl. Phys. **100**, 123912 (2006)
77. J.L. García-Palacios, F.J. Lázaro, Phys. Rev. B **58**, 14937 (1998)
78. S. Giordano, J. Electrost. **58**, 59 (2003)
79. D.R. Brillinger, J. Theor. Prob. **10**, 429 (1997)
80. V. Tulovsky, L. Papiez, Appl. Math. Lett. **14**, 881 (2001)
81. B.J. Berne, R. Pecora, *Dynamic Light Scattering* (Wiley, New York, 1976)
82. P.F. de Châtel, I. Nándori, J. Hakl, S. Mészáros, K. Vad, J. Phys.: Condens. Matter **21**, 124202 (2009)
83. N.W. Ashcroft, N.D. Mermin, *Solid State Physics* (Saunders College, Orlando, 1976)
84. C. Kittel, *Introduction to Solid State Physics*, 7th edn. (John Wiley & Sons, New York, 1996)
85. F. Manca, S. Giordano, P.L. Palla, R. Zucca, F. Cleri, L. Colombo, J. Chem. Phys. **136**, 154906 (2012)
86. F. Manca, S. Giordano, P.L. Palla, F. Cleri, L. Colombo, J. Chem. Phys. **137**, 244907 (2012)
87. M. Abramowitz, I.A. Stegun, *Handbook of Mathematical Functions* (Dover Publication Inc., New York, 1970)